(Received 15 July 2023, Accepted 23 November 2023, Scheduled 7 December 2023)

Effect of Via-Array Side Walls on the Characteristics of SIW Resonator with Novel Design Equations

Samar M. Azab[1], Abdelhamid A. Shaalan[2], Khalid F. A. Hussein[3,*], and Asmaa E. Farahat[3]

[1] *Zagazig Higher Institute of Engineering & Technology, Zagazig, Egypt*
[2] *Electronics and Communication Engineering Department, Faculty of Engineering, Zagazig University, Zagazig, Egypt*
[3] *Microwave Engineering Department, Electronics Research Institute (ERI), Cairo, Egypt*

ABSTRACT: The present work proves by both simulation and experimental work that the most common empirical formulas available in the previous publications for the design of substrate-integrated waveguide (SIW) cavities are incorrect in most cases. Moreover, the present work provides correct and exact design equations that are examined by both simulation and experimental work. In planar circuit structures, rectangular waveguide and resonators are commonly integrated within a dielectric substrate to produce what is known as SIW structures. For ease of fabrication and embedding into the dielectric substrate, the closed (solid) side walls of the rectangular waveguides and resonators are replaced by metallic via arrays. The main concern of the present paper is to investigate the effects of such replacement on the performance of a SIW resonator through simulation as well as experimental work. The limiting constraints on the relative dimensions of such via arrays including the diameter of the vias and the spacing between them are numerically and experimentally investigated to ensure proper operation of the SIW resonator regarding the radiation loss due to leakage from the openings of the resonator side walls. The effects of the via array dimensions on the resonant frequency, radiation loss, and quality factor (Q-factor) of the resonator are evaluated. For this purpose, two models of the rectangular resonator embedded in the dielectric substrate are designed to operate at 10 GHz. The first model is an ideal box-shaped resonator of solid sidewalls whereas the other model is a conventional SIW resonator with via-array side walls. The two types of the substrate-embedded resonators are fed through a microstrip line. The resonant frequency, losses, and Q-factor of the two resonator models are compared to each other taking the box-shaped resonator as a reference because of its ideal structure to evaluate the performance of the conventional SIW resonator. The two types of resonator are fabricated for comparison through experimental measurements. The empirical design equations that are commonly available in literature to calculate the effective dimensions of the SIW resonator are investigated by comparison with the exact simulation results and shown to be incorrect in most cases. More accurate and reliable design equations are proposed in the present work. The results of the proposed design equations are compared to the simulation results showing excellent accuracy and shown to be more reliable than those available in literature.

1. INTRODUCTION

The state-of-the-art wireless communication systems achieve large capacity, high data rates, and require ease of integration of the circuits and components that have low profile, low cost, and low loss. Substrate integrated waveguide (SIW) is an artificial rectangular waveguide implemented in a dielectric substrate material by connecting the top and bottom metal layers using via-holes. The guided waves and characteristic modes are similar to the metallic rectangular waveguide [1]. SIW can be easily integrated with microstrip circuits in the microwave frequency range combining the advantages of waveguide structures and printed planar structures [2]. The present work focuses on the design of a SIW resonator that is a necessary component in many SIW circuits such as resonator filters, cavity-backed slot antennas, slot antenna arrays, and leaky-wave antennas [1–9].

Over the first decade of the present century, the researchers were interested in the formulation of accurate analytic formulas used as design equations for SIW components including interconnects, resonators, filters, and antennas. The effective dimensions are the most important design parameters that require accurate formulas to guide the designer. The work of [10] stated the inequality that determines the range of the effective width of the SIW in terms of distance between the center lines of the via arrays forming the side walls, the diameter of the vias, and the distance between the contiguous vias. The work of [11] proposed an empirical formula to calculate the effective width of the SIW from which the cutoff frequencies of the TE_{10} and TE_{20} modes can be calculated. The work of [12] proposed a formula to be considered as a modification of the empirical formula introduced in [11]. The authors of [13] used the same modified formulas proposed in [12] to investigate the transitions between the microstrip lines and SIW interconnects. The authors of [14] proposed an empirical formula to calculate the effective width of the SIW resonator that was different from the empirical formulas proposed in [11] and [12] and added a new empirical formula to calculate the length of the SIW resonator. The authors of [15] used the same formula proposed in [14] to calculate the effective width of the SIW in order to find analytical equivalence between the SIW and conventional rectangular waveguide. Also, many research studies were interested in calculating the losses in the SIW structures. In [16], a method of analysis was introduced to evaluate the complex propagation

* Corresponding author: Khalid Fawzy Ahmed Hussein (fkhalid@eri.sci.eg).

constant in SIW interconnects so as to calculate the attenuation due to leakage from the side walls of the SIW. The authors of [17] and [18] were interested in the investigation of the different types of losses in the SIW resonators and the evaluation of the resonator Q-factor. Also, the research works of [14, 17–20] were concerned with calculating the Q-factor of the SIW resonators and filters. The work of [13] and [21] introduced design procedure for the SIW interconnects with design equations for the tapered microstrip-to-SIW transitions.

The present work focuses on the design of a SIW resonator and is concerned with introducing a design methodology that enables the designer to arrive at the optimum design of a SIW resonator for a specific purpose. It is shown that the most common empirical formulas available in some publications to calculate the effective width and length of the SIW interconnects and resonators and, hence, to be used as design equations as mentioned above, are not reliable in most of the cases. The present work proposes novel design equations and design procedure for the SIW resonators and subjects these design equations to a stringent test by comparing the results obtained by the proposed formulas to those obtained by the CST simulator and the experimental measurement to evaluate their accuracy.

After the introduction, the principles of the box-shaped resonator are presented in Section 2. The the published and proposed design equations of SIW resonator are presented and discussed in Section 3. The method of feeding the box-shaped SIW resonators with a microstrip line is described in Section 4 with presentation of the design procedure. Section 5 describes the method of calculating the Q-factor of resonator fed with the microstrip line. Section 6 presents the numerical results with detailed discussions. Finally, Section 7 summarizes the conclusions of the present work.

2. RECTANGULAR WAVEGUIDE RESONATOR

Consider a rectangular waveguide filled with a dielectric material of dielectric constant ϵ_r and having the internal dimensions a and b in the x- and y-directions, respectively. The cutoff frequencies of the guided modes are given by the following formula [22] under the assumption that the propagation is in the $+z$-direction.

$$f_{c_{mn}} = \frac{c}{2\pi\sqrt{\epsilon_r}}\sqrt{\left(\frac{m\pi}{a}\right)^2 + \left(\frac{n\pi}{b}\right)^2} \tag{1}$$

where c is the velocity of light in free space; m and n are the mode orders in the x- and y-directions, respectively.

2.1. Resonant Frequency of the Box-Shaped Resonator

A rectangular waveguide (box-shaped) resonator (cavity) is formed by terminating the waveguide in the longitudinal direction ($+z$ direction) by metallic walls at its back ($z = 0$) and front ($z = d$) ends as shown in Figure 1. For a closed waveguide resonator with dimensions a, b, and d, along x, y, and z-coordinates, respectively, the resonant frequency of the mode order m, n, q, in the x-, y-, and z-directions, respectively, is given by the following formula [22].

$$f_{mnl} = \frac{c}{2\pi\sqrt{\epsilon_r}}\sqrt{\left(\frac{m\pi}{a}\right)^2 + \left(\frac{n\pi}{b}\right)^2 + \left(\frac{q\pi}{d}\right)^2} \tag{2}$$

Normally, such a waveguide cavity is box-shaped as shown in Figure 1. If such a resonator is made of perfectly conducting walls and lossless dielectric filler, the resonator is loss-free, and hence, the Q-factor is theoretically infinite.

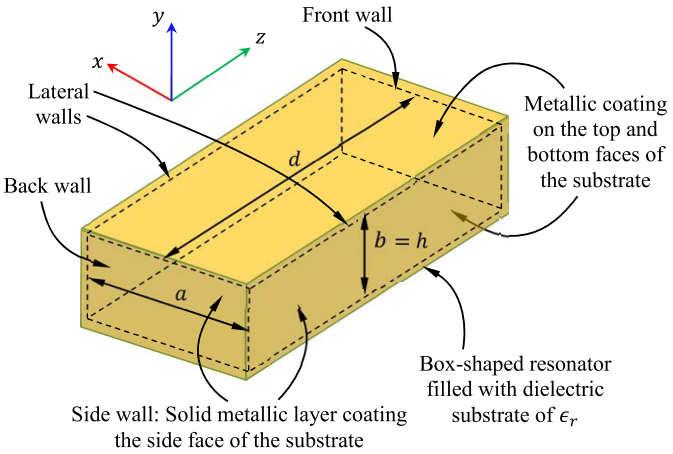

FIGURE 1. Substrate-embedded box-shaped resonator with solid walls.

If such a resonator is to be embedded in a dielectric substrate of thickness h, the height of the waveguide will be the same as the substrate thickness, i.e., $b = h$. Such a dielectric substrate should be double face coated with metallic layers that form the top and faces of the box-shaped resonator. The solid conducting side walls can be added by special fabrication techniques. For example, it can be achieved by cutting the substrate to fit the dimensions of the box-shaped resonator and, then, to coat the side surfaces of the dielectric substrate by metallic layers to construct the side walls of the resonator as solid metallic surfaces. Such a method of fabrication results in a perfectly implemented rectangular waveguide resonator that is actually box-shaped. However, it is difficult to be applied and requires a special technology to coat the side faces of the dielectric substrate with metallic layers. Another way is to insert metallic layers by a special mechanical technique to form the side walls of the resonator as solid metallic faces. It should be noted that in Section 7 of the present work, a method is described to fabricate a box-shaped resonator with solid side walls on a dielectric substrate of material Rogers' RO5880 for comparison with the conventional SIW resonator that is fabricated with via-array side walls on the same substrate material.

2.2. Q-Factor of the Box-Shaped Resonator

The Q factor of a cavity (closed waveguide) resonator can be used as a measure of how long the resonator will sustain free oscillations. Theoretically, a lossless resonator will sustain free oscillations for infinite time. On the other hand, a lossy resonator sustains free oscillations for a finite time duration that depends on the amount of losses. The resonator losses are usually caused by dissipation in the dielectric material filling the cavity of the resonator, Ohmic loss of its electrically conducting

walls, and radiation due to leakage through any existing openings in the resonator walls.

The Q-factor (Q) of a box-shaped resonator with solid metallic walls is not affected by radiation loss and, hence, can be considered as the internal Q-factor (Q_i) that is related to the internal losses of the waveguide resonator (losses of the dielectric filler and the metallic walls). The resonant mode TE_{101} is a first-order resonance in the direction of propagation in the finite-length waveguide, i.e., $q = 1$ in (2). Therefore, at this mode, the waveguide resonator can be considered as a half-wavelength resonator of length L. Such a resonator has an internal Q-factor that can be obtained by the following expression [23].

$$Q = Q_i = \frac{\pi}{2\alpha L} \tag{3}$$

where α is the total attenuation along the resonator due to the losses in the conducting walls and the lossy dielectric filler, and hence, it can be expressed as follows.

$$\alpha = \alpha_d + \alpha_c \tag{4}$$

where α_d and α_c are the attenuation constants due to the dielectric filler and conducting walls, respectively.

The internal Q-factor can be expressed as follows.

$$\frac{1}{Q_i} = \frac{1}{Q_d} + \frac{1}{Q_c} \tag{5}$$

where Q_d and Q_c are the Q-factors attributed to the dielectric filler and conducting walls, respectively, and can be expressed as follows.

$$Q_d = \frac{\pi}{2\alpha_d L} \tag{6a}$$

$$Q_c = \frac{\pi}{2\alpha_c L} \tag{6b}$$

The attenuation constants α_d and α_c in a rectangular waveguide filled with a dielectric material can be calculated using the following formulas [24, 25].

$$\alpha_d = \frac{\pi}{c} f_{101}\sqrt{\epsilon_r}\tan\delta \left[1 - \left(\frac{f_{c10}}{f_{101}}\right)^2\right]^{-\frac{1}{2}} \tag{7a}$$

$$\alpha_c = \frac{R_s\sqrt{\epsilon_r}}{120\pi h}\left[1+\frac{2h}{W}\left(\frac{f_{c10}}{f_{101}}\right)^2\right]\left[1-\left(\frac{f_{c10}}{f_{101}}\right)^2\right]^{-\frac{1}{2}} \tag{7b}$$

where $\eta_d = \sqrt{\mu_d/\epsilon_d}$; μ_d, ϵ_d, and $\tan\delta$ are the permeability, permittivity, and loss tangent of the dielectric filler; f_{c10} is the cutoff frequency of the TE_{10} mode and can calculated by (1); f_{101} is the resonant frequency of the TE_{101} mode and can be calculated by (2); R_s is the surface resistance of the conducting walls and can be calculated as follows [24, 25].

$$R_s = \sqrt{\frac{\pi\mu_c f_{101}}{\sigma_c}} \tag{8}$$

where μ_c and σ_c are the permeability and conductivity of the metallic walls material.

3. SIW WAVEGUIDE RESONATOR

When a rectangular waveguide resonator is to be embedded into a dielectric substrate, it can be implemented using solid metallic walls to form the side walls (front, back, and lateral walls) to take the same form of a box-shaped resonator as shown in Figure 1. However, as mentioned before, this method is difficult to be implemented as it needs special fabrication facilities. The alternative method to implement such a resonator is to replace the solid side walls ( ) by arrays of metallic vias as shown in Figure 2. Regarding such a method of SIW resonator fabrication, the implementation of the via-array sidewalls is simpler than the implementation of the solid walls due to the available conventional printed-circuit-board fabrication facilities. The main drawback of this method of implementation is the unavoidable radiation loss associated with the periodic openings of the side walls due to the leakage of the electromagnetic power through the spacing between the vias.

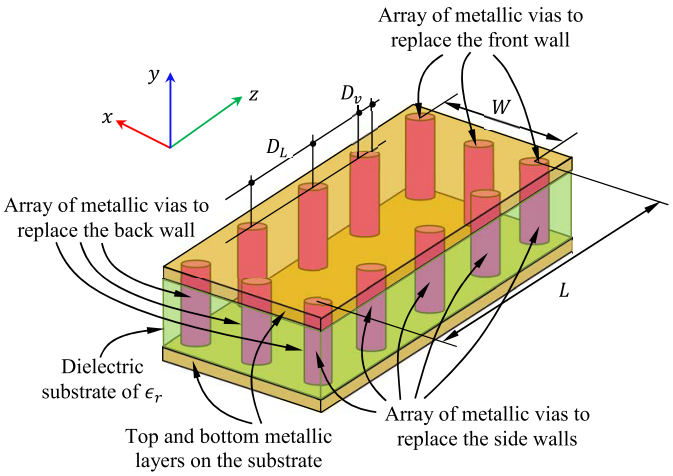

FIGURE 2. SIW waveguide resonator embedded in a dielectric substrate to form a SIW rectangular resonator with via-array side walls.

3.1. Effective Dimensions of the SIW Resonator

For a box-shaped resonator with solid side walls, Figure 1, of internal dimensions $W \times h \times L$, the resonant frequencies can be calculated by formula (1) using $a = W$, $b = h$, and $d = L$. However, for a SIW resonator with via-array side walls, Figure 2, to calculate the same resonant frequency for a specific mode (m, n, q) using formula (1), the parameters a and d should be substituted with effective values as there is no real values that can be assigned to the width or length of the resonator. Thus, the following substitutions are to be performed to calculate the resonant frequency given by formula (1).

$$a = W_{eff}, \quad b = h, \quad d = L_{eff} \tag{9}$$

Empirical formulas to calculate the values of W_{eff} (and, similarly, for L_{eff}) are supplied in many published papers such as [11, 12, 17, 26]. These formulas are given as follows.

$$W = W_{eff} + \frac{D_v^2}{0.95 D_L} \tag{10a}$$

$$L = L_{eff} + \frac{D_v^2}{0.95 D_L} \tag{10b}$$

Other formulas resulting from modifying (9) to improve the accuracy are given as follows [12, 13, 26].

$$W = W_{eff} + 1.08\frac{D_v^2}{D_L} - 0.1\frac{D_v^2}{W} \quad (11a)$$

$$L = L_{eff} + 1.08\frac{D_v^2}{D_L} - 0.1\frac{D_v^2}{W} \quad (11b)$$

Also, other different formulas are given in [14, 15, 26] as follows.

$$W = \frac{2W_{eff}}{\pi}\cot^{-1}\left(\frac{\pi D_L}{4W_{eff}}\ln\frac{D_L}{2D_v}\right) \quad (12a)$$

$$L = \frac{2L_{eff}}{\pi}\cot^{-1}\left(\frac{\pi D_L}{4L_{eff}}\ln\frac{D_L}{2D_v}\right) \quad (12b)$$

3.2. Q-Factor of the SIW Resonator

The Q-factor of a rectangular resonator is affected by the losses inside the resonator. The higher the losses in the resonator are, the lower its Q-factor is. In addition to the Ohmic losses of the conducting walls and the dielectric material in a SIW resonator with via-array side walls, the separation between the vias may cause some leakage of the stored energy to the external region, thereby leading to reducing the Q-factor. Actually, the Q-factor is meaningful only for low-loss cavities; the Q-factor of a high-loss resonator does not make sense. Thus, comparing the Q-factor of a box-shaped resonator (of solid side walls) with that of a SIW resonator (of via-array side walls), when both are embedded in a substrate of the same type, can give information about the recommended via-array dimensions to keep the Q-factor as high as possible or to realize a specific bandwidth when the resonator is used in a filter.

As mentioned before, SIW resonator can be seen as a finite-length waveguide with via-array terminating walls at the back and front ends in addition to those of the lateral walls as shown in Figure 2. Thus, the losses in such a cavity can be evaluated by calculating the attenuation over the cavity length (in the direction of propagation) and then calculating the losses as the multiplication of the total attenuation constant by the length of the cavity. In addition to the attenuation constant α_c caused by the Ohmic loss due to the finite conductivity of the metallic walls and the attenuation constant α_d caused by the dielectric loss due to the non-zero conductivity of the dielectric material filling the interior of the SIW resonator, the radiation loss exists due to electromagnetic leakage from the separation between the vias of the side walls. Thus, the total attenuation constant, α, in a SIW with via-array side-walls can be evaluated as follows [23].

$$\alpha = \alpha_d + \alpha_c + \alpha_r \quad (13)$$

where α_r is the attenuation constant due to the leakage from openings in the side walls.

Consequently, the Q-factor of the SIW resonator with via-array side-walls can be evaluated as follows [22].

$$\frac{1}{Q} = \frac{1}{Q_i} + \frac{1}{Q_r} = \frac{1}{Q_d} + \frac{1}{Q_c} + \frac{1}{Q_r} \quad (14)$$

where Q_i and Q_r are the internal and external Q-factors, respectively. The internal Q-factor, Q_i, can be evaluated by (5) in the same way as described in Subsection 2.2. The external Q-factor is related to the radiation loss caused by leakage through the via-array side walls. The value of Q_r is related to attenuation constant α_r caused by radiation as follows [22].

$$Q_r = \frac{\pi}{2\alpha_r L} \quad (15)$$

Thus, to evaluate Q_r, the attenuation constant α_r should be determined. A method is proposed in [16] to evaluate the complex propagation constant in a SIW interconnect from which α_r can be estimated. The work of [18] presents some numerical results for the radiation loss. However, the methods of analysis presented in both [16] and [18] do not provide direct method for evaluating the attenuation constant α_r.

4. RECTANGULAR WAVEGUIDE RESONATOR FED WITH MICROSTRIP LINE

As mentioned above, when a rectangular waveguide resonator is to be embedded in a double-side-coated substrate, it can be fabricated either with solid side walls to produce a box-shaped resonator as shown in Figure 1 or by the conventional way using arrays of metallic vias to replace the side walls as shown in Figure 2. The fabricated SIW resonators are fed through microstrip lines as shown in Figures 3 and 4. The box-shaped rectangular waveguide resonator shown in Figure 3 has no radiation loss due to its solid walls, and therefore, it is used in the present work as a reference to investigate the effects of the via array side walls on the performance of the SIW resonator shown in Figure 4.

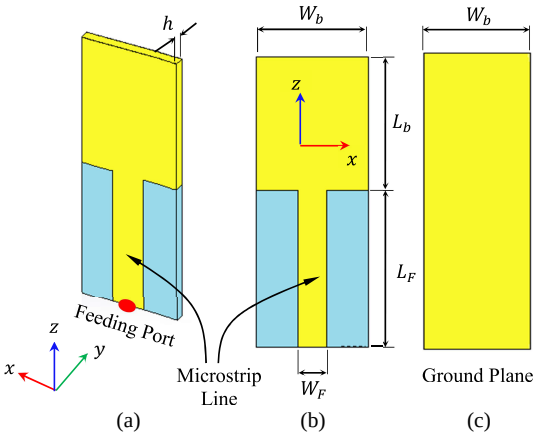

FIGURE 3. Box-shaped rectangular resonator with solid side walls embedded in a dielectric substrate. (a) 3D view. (b) Top view. (c) Bottom view.

4.1. Box-Shaped Resonator Fed with Microstrip Line

The box-shaped resonator can be embedded in a dielectric substrate and fed through a microstrip line as shown in Figure 3. The dimensions of the cavity can be set so that this resonator is excited in the resonant mode TE_{101} at the desired frequency f_{101} given by (2) with $m = 1$, $n = 0$, and $q = 1$. At resonance,

the resonator impedance is pure real and can be easily matched to $50\,\Omega$. The characteristic impedance of a quarter-wavelength microstrip line ($\lambda/4$ transformer) can be determined to realize the required impedance matching. Thus, the width of the microstrip line, W_F, can be, simply, set to match the resonator impedance to $50\,\Omega$.

A box-shaped resonator of solid walls with the dimensions listed in Table 1 has its first-order internal resonance (TE_{101}) at 10 GHz. Extensive parametric studies have been performed using the commercially available CST® simulator to arrive at the dimensions that give $f_{101} = 10$ GHz exactly. This resonator is taken as a reference for the comparison with the SIW resonator of via-array side walls whose design is described in the next subsection.

TABLE 1. Dimensions of a box-shaped resonator with solid side walls embedded in a dielectric substrate of height h and $\epsilon_r = 2.2$ to resonate at 10 GHz.

Parameter	W_b	L_b	h	W_F	L_F
Value (mm)	16.517	12.437	1.57	3.62	19.2

4.2. SIW Resonator Fed with Microstrip Line

The SIW resonator with via-array side walls can be embedded in a dielectric substrate and fed through a microstrip line as shown in Figure 4. The dimensions of the SIW cavity are set to excite the resonant mode TE_{101} in the cavity at the desired frequency f_{101}. In the design process, formula (2) and the SIW design equations proposed in the present work (see Section 5) can be used to determine the values of the dimensional parameters shown in Figure 4 to get f_{101} equal to the desired value. The electromagnetic simulation can, then, be used for fine tuning of these dimensions to realize the exact value of the desired resonant frequency. At resonance, the resonator impedance is pure real and can be easily matched to $50\,\Omega$. The length of the microstrip line is $1/4\lambda_g$; where λ_g is the guided wavelength of the microstrip line at 10 GHz.

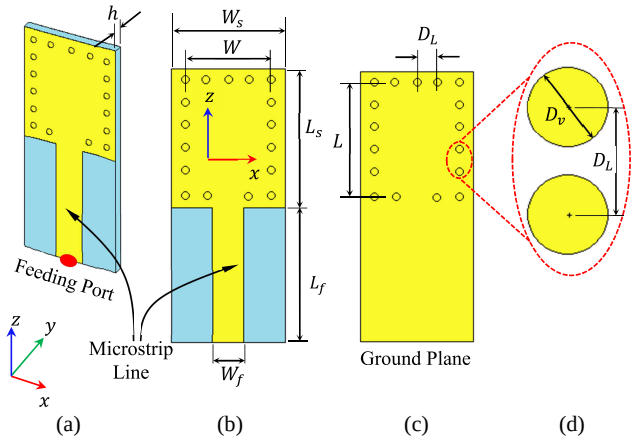

FIGURE 4. SIW rectangular resonator with via-array side walls embedded into a dielectric substrate of height h and $\epsilon_r = 2.2$. (a) 3D view. (b) Top view. (c) Bottom view. (d) Zoom-in view.

The width of the microstrip line, W_F, should be set to match the resonator impedance to $50\,\Omega$. The SIW resonator of the design shown in Figure 4 is to be numerically investigated in Section 6 taking the box-shaped resonator shown in Figure 3 as a reference for subjective (and fair) comparative performance assessment. The effects of the dimensions of the via-array side walls (D_v and D_L) on the characteristics of the SIW cavity are to be investigated through simulation and measurement. Furthermore, the empirical formulas (9), (10), (11), and (12) are to be examined by comparing the values of the resonant frequency obtained by these empirical formulas when substituted into formula (2) to those obtained by simulation. Also, the design Equations (13) proposed in the present work are examined versus the published formula.

Extensive parametric study has been performed using the commercially available CST® simulator to arrive at the dimensions of the SIW resonator listed in Table 2 so as to get its first resonance $f_{101} = 10$ GHz.

5. PROPOSED DESIGN FORMULAS FOR THE EFFECTIVE DIMENSIONS OF THE SIW RESONATOR

In this section, the results obtained by the empirical formulas (10) and (12) proposed in [11, 12] and [14, 15], respectively, for the dependence of the resonant frequency f_{101} on D_L and D_v are compared to the exact results obtained by the CST® simulator. It is shown by this comparison that both the design formulas (10) and (12) have inadequate accuracy to calculate the dimensions of the SIW resonator so as to resonate at a required frequency. The present work suggests more accurate formulas to calculate the effective width and length of the SIW resonator. The numerical results presented in this section show that the formulas proposed in the present work are accurate and reliable as design equations for the SIW resonators and interconnects.

5.1. Assessment of the Published Design Formulas of the SIW Resonator

One of the objectives of the present work is to investigate the validity and accuracy of the empirical formulas (10) and (12) when used as design equations of the SIW components including interconnects, resonators, and filters. For this purpose, the resonant frequency, f_{101}, of a SIW cavity with the dimensions given in Table 2 is evaluated using the CST® simulator for varying values of D_v and D_L. On the other hand, the resonant frequency, f_{101}, is obtained by the empirical formulas (10) and (12) proposed in [11, 12] and [14, 15], respectively. The comparisons between the values of f_{101} obtained by the CST® simulator and those obtained by the mentioned empirical formulas are presented in Figure 5. It is shown that the values of f_{101} obtained by the empirical formulas (10) and (12) are either inaccurate or incorrect compared to the corresponding exact values obtained by the CST® simulator.

5.2. Method of Construction of Accurate Design Formulas of the SIW Resonator

It is noticed in Figure 5 that the slope of the D_L-f_{101} curves given by the empirical formula (10) is much lower than that of the corresponding exact curve obtained by simulation whereas the slope of the corresponding curve given by the empirical

TABLE 2. Dimensions of a SIW resonator with via-array side walls embedded into a dielectric substrate of height h and $\epsilon_r = 2.2$ to resonate at 10 GHz.

Parameter	W	L	h	D_v	D_L	W_s	L_s	W_F	L_F
Value (mm)	16.517	12.437	1.57	0.4	1.5	18.517	14.437	3.64	17.7

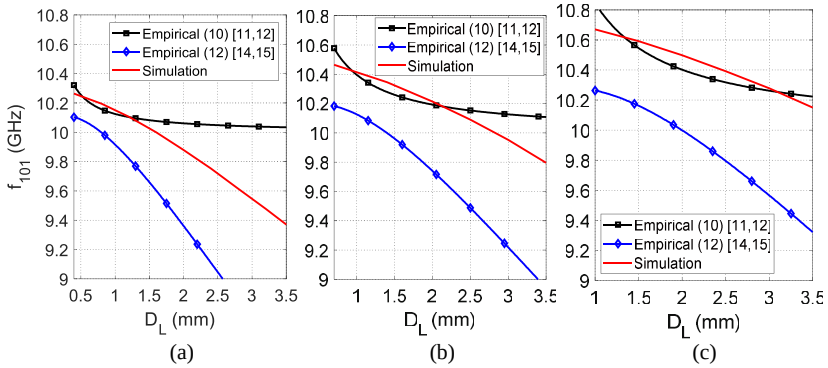

FIGURE 5. Comparison between the results of simulation and empirical formulas (10) and (12) for the dependence of the resonant frequency f_{101} of the SIW resonator on the separation D_L between the vias for (a) $D_v = 0.4$ mm, (b) $D_v = 0.7$ mm, (c) $D_v = 1$ mm.

formula (12) is much higher than that obtained by simulation. Therefore, it may be appropriate to propose a new empirical formula that gives a D_L-f_{101} curve running between those obtained by (10) and (12). Thus, it is suggested to construct a new empirical formula by merging (10) and (12) using some weighting coefficients as follows. The term on the right-hand side of (12) is added to the second term on the right-hand side of (10), and then, unknown weighting factors, a_1, b_1, c_1, d_1, a_2, b_2, c_2, and d_2, are used to construct the merged empirical formula as follows.

$$W = a_1 W_{eff} \cot^{-1}\left(b_1 \frac{D_L}{W_{eff}} \ln c_1 \frac{D_L}{D_v}\right) + d_1 \frac{D_v^2}{D_L} \quad (16a)$$

$$L = a_2 L_{eff} \cot^{-1}\left(b_2 \frac{D_L}{L_{eff}} \ln c_2 \frac{D_L}{D_v}\right) + d_2 \frac{D_v^2}{D_L} \quad (16b)$$

To evaluate the unknown eight unknown coefficients a_1, b_1, c_1, d_1, a_2, b_2, c_2, and d_2, the particle swarm optimization (PSO) is applied with the optimization goal of minimizing the error between the values of the resonant frequency, $f_{101_{Emp}}$, obtained by the constructed empirical formula and the corresponding values, $f_{101_{Sim}}$, obtained by the CST® simulator. Accordingly, the cost function of the PSO algorithm can be expresses as follows.

$$F_{Cost} = f_{101_{Emp}} - f_{101_{Sim}} \quad (17)$$

The application of the PSO algorithm is achieved through a Matlab® program developed by the authors for the purpose of calculating the optimum values of the unknown coefficients in (16). The PSO algorithm runs iteratively to arrive at the following optimum values of these unknown coefficients.

$$a_1 = a_2 = \frac{2}{\pi} \quad (18a)$$

$$b_1 = b_2 = \frac{\pi}{6} \quad (18b)$$

$$c_1 = c_2 = \frac{1}{4} \quad (18c)$$

$$d_1 = d_2 = \frac{1}{3} \quad (18d)$$

By substitution from (18) into (16), the final forms of the proposed empirical formulas are given by (19).

$$W = \frac{2W_{eff}}{\pi} \cot^{-1}\left(\frac{\pi D_L}{6W_{eff}} \ln \frac{D_L}{4D_v}\right) + \frac{D_v^2}{3D_L} \quad (19a)$$

$$L = \frac{2L_{eff}}{\pi} \cot^{-1}\left(\frac{\pi D_L}{6L_{eff}} \ln \frac{D_L}{4D_v}\right) + \frac{D_v^2}{3D_L} \quad (19b)$$

It is shown through the numerical investigations presented in Section 5.3 that the proposed empirical formulas (19) are more accurate design equations that can be used to calculate the width and length of the SIW resonator (for a desired value of f_{101}) compared to those given by (10) and (12).

5.3. Investigation of the Accuracy of the Empirical Formulas for the Effective Dimensions of the SIW Resonator

One of the aims of the present work is to investigate the validity of the empirical formulas (10) and (12) proposed in [11, 12] and [14, 15], respectively, to be used as design equations of the SIW components and presented in many other publications such as [13, 17, 26]. In the meanwhile, it is required to investigate the design equations (19) proposed in the present work for the design of the SIW resonator. For this purpose, the curves plotted in Figure 12 are presented and compared to each other. The horizontal-line (at 10 GHz) is demonstrated as a reference curve and represents the resonant frequency f_{101} of a box-shaped resonator with the dimensions listed in Table 1. The dimensions of the SIW resonator with via-array side walls are set equal to the dimensions of the box-shaped resonator, i.e., $W = W_b = 16.517$ mm, $L = L_b = 12.437$ mm, and

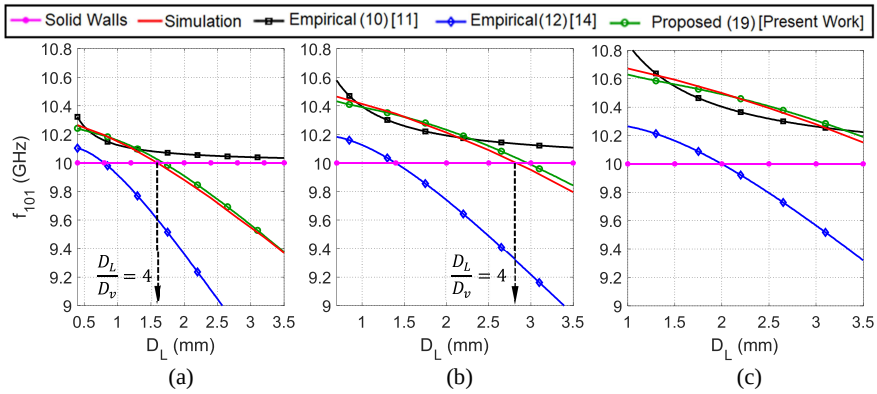

FIGURE 6. Comparison between the results of simulation and empirical formula for the dependence of the resonant frequency f_{101} of the SIW resonator on the separation D_L between the vias for (a) $D_v = 0.4$ mm, (b) $D_v = 0.7$ mm, (c) $D_v = 1$ mm.

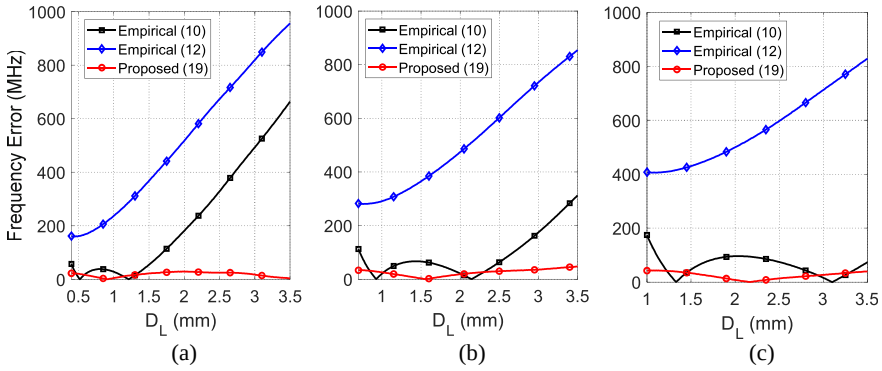

FIGURE 7. Dependence of the absolute errors of the resonant frequency f_{101} of the SIW resonator on the separation D_L between the vias when the design equations (10), (12), and (19) are used. (a) $D_v = 0.4$ mm, (b) $D_v = 0.7$ mm, (c) $D_v = 1$ mm.

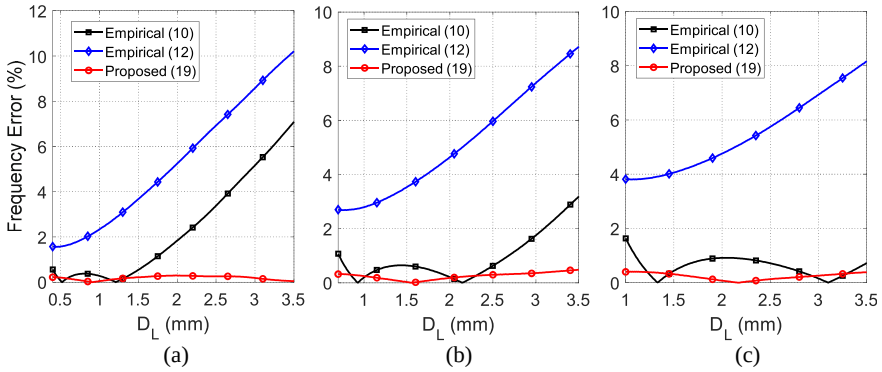

FIGURE 8. Dependence of the percent errors of the resonant frequency f_{101} of the SIW resonator on the separation D_L between the vias when the design equations (10), (12), and (19) are used. (a) $D_v = 0.4$ mm, (b) $D_v = 0.7$ mm, (c) $D_v = 1$ mm.

$h = 1.57$ mm. The curves of the resonant frequency, f_{101}, calculated by formula (2) by setting $a = W_{eff}$, $b = h$, and $d = L_{eff}$ after using each of (10), (12), and (19) to calculate the values of W_{eff} and L_{eff} with varying D_L are presented in Figure 12 for different values of D_v. To examine their accuracy, the curves obtained by the mentioned design equations are compared to the corresponding curves obtained by the CST® simulator. From the curves presented in Figure 6, it is found that the effective width and length of the SIW resonator obtained from Equations (10) and (12) are inaccurate when used to evaluate the resonant frequency, f_{101}, of this resonator using expression (2). Moreover, the resonant frequency obtained by (10) is much different from that obtained by (12). It is shown that the results obtained by the CST® simulator for the resonant frequency of SIW resonator are significantly different from those obtained by these empirical formulas or the design equations. The dependences of the absolute and percent errors of the resonant frequency f_{101} of the SIW resonator obtained by the design equations (10), (12), and (19) on the separation D_L between the vias are presented in Figures 7 and 8, respectively, for differ-

ent values of the via diameter D_v. It is shown that the design equation (19), proposed in the present work, has the best accuracy and results in the minimum error of the resonant frequency compared to the results obtained by the design equations (10) and (12). Also, it is clear that the error of the resonant frequency obtained by (10) and (12) increases with increasing D_L and decreasing D_v. On the other hand, the resonant frequency calculated using the effective dimensions obtained by expression (19), proposed in the present work, is found to be very close to that obtained by the CST® simulator at all the values of D_v and D_L. It is shown that the percent error of the resonant frequency f_{101} obtained by the design equations (19) does not exceed 0.3% in all the cases.

It is noticeable from the behavior of the resonant frequency with varying the via-array dimensions, D_v and D_L, that $W_{eff} < W$ and $L_{eff} < L$ for $D_L/D_v < 4$ and that $W_{eff} > W$ and $L_{eff} > L$ for $D_L/D_v < 4$. This will be discussed more in view of the fringing of the field outside the cavity of the SIW resonator with increasing the distance between the vias in Section 7.6. It means that the ratio D_L/D_v has a critical value of 4, and at this value, the field fringes outside the SIW resonator, hence, the radiation loss has drastic changes

6. Q-FACTOR OF SIW RESONATOR FED THROUGH MICROSTRIP LINE

As the resonator is not a radiating element, the unique mechanism to couple the power from the source to the interior of the resonator through the microstrip line is the resonance mechanism. Only at the resonant frequencies of the cavity, the reflection coefficient at the excitation port at the beginning of the microstrip line shown in Figures 3 and 4 has very sharp minima with very narrow bands. Theoretically, for a lossless resonator, the bandwidth of impedance matching at resonance tends to zero.

The performance of the SIW resonator excited in the resonant mode TE_{101} can be investigated through calculating the power transmitted into the resonator over a narrow band of the frequencies around the resonant frequency, f_{101}. The ratio of the power absorbed into the SIW resonator (at resonance) to the total input power through a quarter-wavelength microstrip line impedance transformer that plays the role of complete impedance matching between the resonator and the feeding source is equal to the squared magnitude of the transmission coefficient, T, and can be expressed as follows [22].

$$|T|^2 = 1 - |S_{11}|^2 \tag{20}$$

where S_{11} is the reflection coefficient at the feeding port under the assumption of complete impedance matching between the resonator and feed line at the resonant frequency.

The Q-factor of the resonator is then calculated from the frequency response of $|T|$ as follows [22, 23].

$$Q = \frac{f_{101}}{\Delta f} \tag{21}$$

where f_{101} is the resonant frequency of the TE_{101} mode, and Δf is the half-power ($|T| = -3$ dB) bandwidth of the resonator at resonance and defined as follows.

$$\Delta f = f_2 - f_1 \tag{22}$$

where f_1 and f_2 are the lower and upper frequencies of the frequency band within which $|T| \geq -3$ dB.

Under the assumption that the SIW resonator of via-array side walls is made of lossless material, i.e., perfectly conducting metal and ideal dielectric, the losses may be caused only by radiation (leakage) through the openings between the vias forming the sidewalls. Therefore, it is expected that the Q-factor of the SIW resonator will be lower than that of the box-shaped resonator. The difference of the Q-factor between the two types of resonator will increase with increasing the separation between the vias. For this reason, the box-shaped resonator is used as an ideal reference for comparative analysis of the SIW resonator.

7. NUMERICAL INVESTIGATION OF THE EFFECT OF THE VIA-ARRAY SIDE WALLS ON THE CHARACTERISTICS OF THE SIW RESONATOR

This section is concerned with the presentation of the numerical results about the effects of the via-array side wall dimensions on the SIW cavity resonator. These dimensions include the diameter of the vias and the separation between them. The numerical results are concerned with the investigation of the validity and accuracy of closed form empirical formulas available in the literature for calculating the effective dimensions of the SIW resonator. Also, the design equations proposed in the present work are examined versus the published formulas, and the results of the comparative analysis are discussed.

7.1. Effect of the Via-Array Dimensions on the Frequency Response of the SIW Resonator

The fractional power absorbed by the SIW resonator is equal to the square of the magnitude of the transmission coefficient $|T|^2$, where $|T|$ is the magnitude of the transmission coefficient at the feeding port of a SIW resonator and has expression (20) in terms of the reflection coefficient magnitude, $|S_{11}|$. Figure 9 presents the frequency response of $|T|$ for a SIW resonator with the dimensions listed in Table 2 for different values of the separation D_L between the vias. It is shown that the resonant frequency decreases as D_L increases. Also, it is noticeable that the bandwidth is increased, i.e., the Q-factor of the resonator is decreased, with increasing D_L. This can be attributed to the increase of the resonator radiation loss due to electromagnetic leakage (i.e., radiation) through the openings of the side walls with increasing the separation between the vias. Also, it is noticeable that increasing the diameter of the vias, D_v, leads to increasing the Q-factor of the resonator due to the reduction of the separating spaces between the vias, which reduces the radiation loss.

7.2. Effect of the Via-Array Dimensions on the Resonant Frequency of the SIW Resonator

To investigate the effects of the dimensions of the via-array sidewalls of the SIW resonator on the frequency response of the power absorbed by the resonator while being excited in the res-

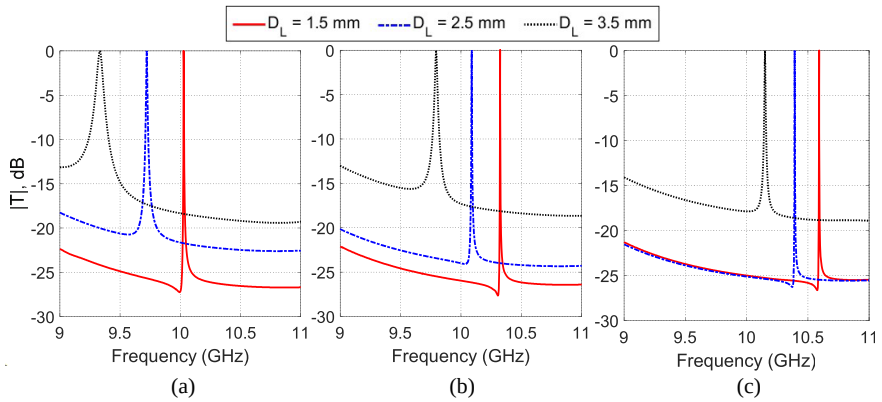

FIGURE 9. Frequency response of the fractional power absorbed by a SIW resonator of lossless material for different values of the separation, D_L, between the vias. The via diameter is set to (a) $D_v = 0.4$ mm, (b) $D_v = 0.7$ mm, (c) $D_v = 1.0$ mm.

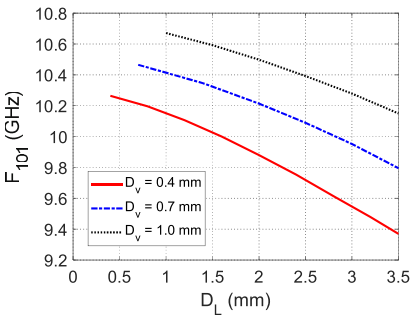

FIGURE 10. Dependence of the resonant frequency of the resonance mode TE_{101} for a SIW resonator of lossless material on the distance D_L between the vias for different values of the via diameter, D_v. The curves are obtained by simulation.

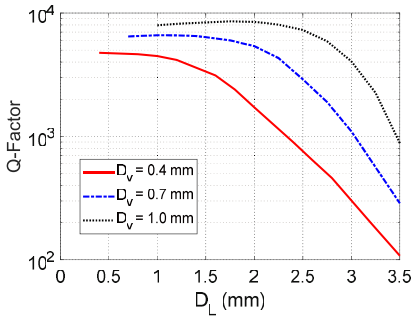

FIGURE 11. Variation of the Q-factor of the resonance mode TE_{101} for a SIW resonator of lossless material with varying the diameter, D_v, of the vias and the separation, D_L, between them. The SIW is fed through a microstrip line as shown in Figure 4. The other dimensions of the resonator are given in Table 2.

onance mode TE_{101}, the curves presented in Figure 10 are plotted. It is shown that the resonant frequency, f_{101}, of the SIW resonator decreases with increasing the separation D_L between the vias for different values of the via diameter, D_v. This can be interpreted as that increasing the distance between the vias leads to increasing the fringing of the cavity fields (as explained later on) which has the same effect of increasing the effective dimensions of the resonator, thereby leading to decreasing the resonant frequency. Also, it is noticeable that increasing the diameter of the vias, D_v, leads to increasing the resonant frequency as it reduces the effective dimensions of the cavity according to (19) and, also, due to the reduction of the separating spaces between the vias, which limits the fringing fields.

7.3. Effect of the Via-Array Dimensions on the Q-Factor of the SIW Resonator

To account only for radiation loss through the side walls of a SIW resonator, it is considered that the resonator is made of lossless materials, i.e., ideal dielectric ($\delta_d = 0$) and perfect electric conductor ($\sigma_c \to \infty$). Under these considerations, the simulation results give the dependence of the Q-factor ($Q = Q_r$) on the via diameter, D_v, and the distances between vias, D_L, as shown in Figure 11. It is evident that the Q-factor of such a resonator decreases with increasing the spacing, D_L, between the vias. It means that the electromagnetic power leakage from the resonator through the openings of the side walls increases with increasing D_L. Thus, to maintain the Q-factor of the SIW resonator as high as possible, the separation between the vias should be minimized. However, due to mechanical constraints, the separation between the vias cannot be decreased below a limit that reserves the mechanical robustness of the final structure. Also, it is noticeable that the Q-factor decreases with decreasing the diameter, D_v, of the vias for the same value of the spacing D_L.

7.4. Effect of Dielectric Losses on the Quality Factor of the SIW Resonator

By taking the dielectric loss into consideration, the dependence of the Q-factor of the SIW resonator of via-array side-walls on the dielectric loss ($\tan\delta$), as obtained by simulation, is presented in Figure 12 for different values of the distance D_L between the vias. It is shown that for small spacing between the vias, the Q-factor is dominated by the dielectric loss whereas, for large separation between the vias, and the resonator Q-factor is dominated by the leakage loss due to the radiation from the openings of the side-walls.

For understanding the behavior of the Q-factor of the SIW resonator as presented in Figure 12 with varying $\tan\delta$ and D_L,

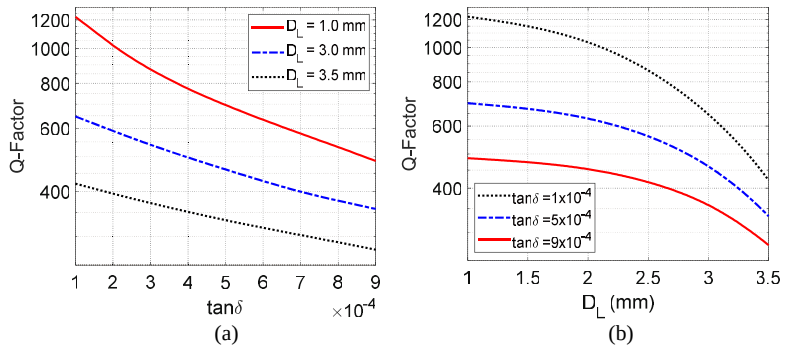

FIGURE 12. Variation of the Q-factor of a SIW resonator of the dimensions listed in Table 2 (except that $D_v = 1.0\,\text{mm}$) with varying (a) the loss tangent, $\tan\delta$, of the dielectric substrate and (b) the spacing, D_L, between the vias.

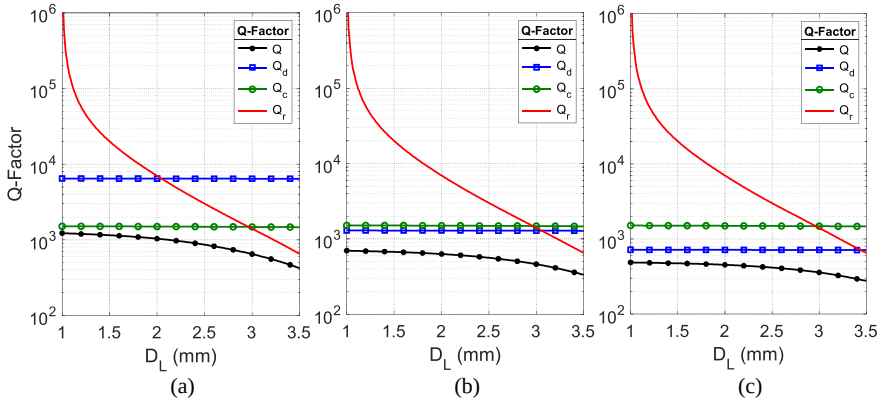

FIGURE 13. Dependence of the components of the Q-factor (Q_d, Q_c, and Q_d) on the spacing, D_L, between the vias for a SIW resonator of lossy materials and having the dimensions listed in Table 2 (with $D_v = 1.0\,\text{mm}$). (a) $\tan\delta = 0.0001$. (b) $\tan\delta = 0.0005$. (c) $\tan\delta = 0.0009$.

the dependences of the components of the net Q-factor (Q_d, Q_c, and Q_r) on the spacing, D_L, between the vias for different values of $\tan\delta$ are presented in Figure 13. The SIW resonator under investigation is made of lossy materials and has the dimensions listed in Table 2 (except that $D_v = 1.0\,\text{mm}$). It should be noted that the factors Q_d and Q_c are calculated using (6). The net Q-factor, Q is obtained by the CST® simulator using the method presented in Section 5. The component of the Q-factor related to the radiation loss, Q_r, is calculated as follows.

$$Q_r = \left(\frac{1}{Q} - \frac{1}{Q_d} - \frac{1}{Q_c}\right)^{-1} \tag{23}$$

The dependence of the attenuation constants α_d, α_c, and α_r of the same resonator on the distance D_L between the vias for different values of $\tan\delta$ are presented in Figure 14. It should be noted that α_d and α_c are calculated using (7) whereas α_r is calculated from Q_r using (20).

It is shown that, for a dielectric material of $\tan\delta = 0.0009$, the dielectric loss is much higher than the conductor loss and is higher than the radiation loss for all the values of D_L; therefore, when $\tan\delta = 0.0009$, the component Q_d dominates as the main component of the net Q-factor (Q). For a dielectric material of $\tan\delta = 0.0005$, the dielectric loss is considerably reduced and becomes very close to the conductor loss, and both of them are higher than the radiation loss for $D_L < 3\,\text{mm}$. Therefore, the components Q_d and Q_c dominate for $D_L < 3\,\text{mm}$, whereas Q_r dominates for $D_L > 3\,\text{mm}$. For a dielectric material of $\tan\delta = 0.0001$, the dielectric loss is further reduced and becomes much lower than the conductor loss and, hence, Q_d becomes much higher than Q_c. Therefore, Q_c is the dominant component of the net Q-factor for $D_L < 3\,\text{mm}$, whereas the radiation loss increases with increasing D_L, and hence, Q_r dominates for $D_L > 3\,\text{mm}$.

7.5. Keeping the Resonant Frequency of the SIW Resonator Fixed While Varying the Via-Array Dimensions

The monotonic decrease of the resonant frequency, f_{101}, with increasing D_L, as shown in Figure 10, can be interpreted as that increasing the separation between the vias has the effect of increasing the effective dimensions of the SIW resonator thereby reducing the resonant frequency of the resonator as discussed before. To maintain the resonant frequency fixed at 10 GHz while the separation D_L is being increased, the resonator dimensions W and L should be decreased so as to compensate the increase of the effective resonator dimensions with increasing D_L. The other dimensions of the transmission line and the substrate are kept the same as those listed in Table 2. Figure 15 presents the frequency response of the fractional power absorbed by a SIW resonator around the TE_{101} resonance for different values of the separation D_L between the vias. The via diameter is set to $D_v = 0.7\,\text{mm}$. The resonator dimensions W

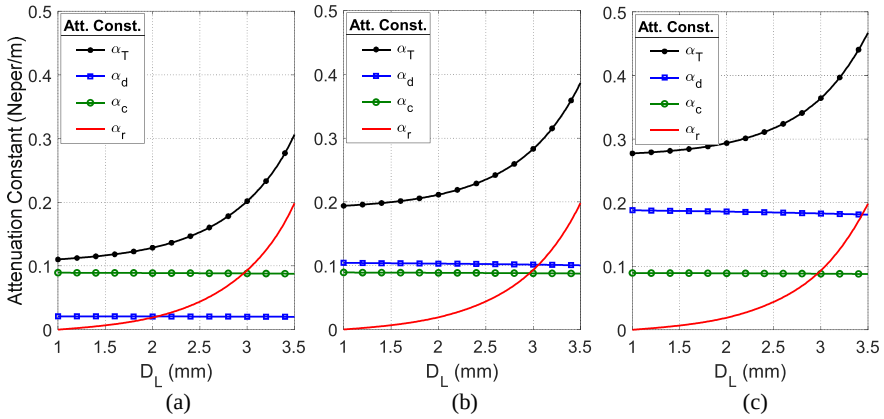

FIGURE 14. Dependence of the attenuation constants (α_d, α_c, and α_d) on the spacing, D_L, between the vias for a SIW resonator of lossy materials and having the dimensions listed in Table 2 (with $D_v = 1.0\,\text{mm}$). (a) $\tan\delta = 0.0001$. (b) $\tan\delta = 0.0005$. (c) $\tan\delta = 0.0009$.

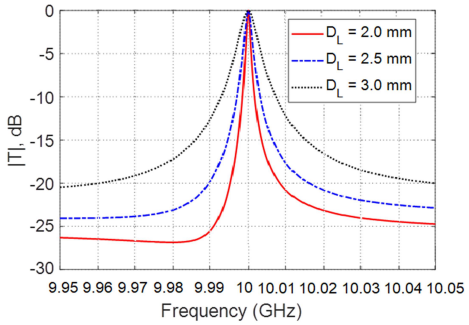

FIGURE 15. Frequency response of the fractional power absorbed by a SIW resonator of lossless material with the dimensions listed in Table 2 (except that $D_v = 0.7\,\text{mm}$) for different values of the separation D_L between the vias. The dimensions W and L are changed as listed in Table 3 to maintain the resonant frequency fixed at 10 GHz.

TABLE 3. Q-factor of the SIW cavities with the frequency responses presented in Figure 15 while varying the SIW resonator dimensions W and L to maintain the resonant frequency fixed at 10 GHz.

Spacing D_L	Resonator Dimensions		Q-factor
	W	L	
2.0 mm	16.51 mm	12.44 mm	5329
2.5 mm	16.34 mm	12.16 mm	2869
3.0 mm	16.14 mm	12.06 mm	1223

and L are changed as listed in Table 3 to maintain the resonant frequency fixed at 10 GHz. However, as shown in Figure 15 and Table 3, the Q-factor is decreased with increasing the separation D_L due to the increase of the power leakage (radiation) through the side walls of the SIW resonator with increasing D_L.

7.6. Explanation of the Effective Dimensions of the SIW Resonator in View the Fringing Field

Normally, the electric field of the resonance mode TE_{101} of a box-shaped resonator is completely confined inside the resonator cavity and is vertically oriented (i.e., it has only E_y-component parallel to the side walls). With increasing the distance D_L between the vias, the intensity of the field inside the cavity is reduced due to the increase of the radiation loss. This is shown by comparing the field distributions presented in Figures 16(a) and 17(a) ($D_L/D_v = 2$) to that presented in Figures 16(b) and 17(b) ($D_L/D_v = 7$) for $D_v = 0.4\,\text{mm}$. For wide separation between the vias ($D_L = 2.8\,\text{mm}$), when D_v is increased, the field intensity inside the cavity of the SIW resonator increases again as shown by the field distribution in Figures 16(c) and 17(c) in comparison to that shown in Figures 16(b) and 17(b).

For relatively narrow separation between the vias constructing the side walls of a SIW resonator ($D_L/D_v < 4$), the electric field is almost confined inside the side walls without fringing and is similar to that of the box-shaped resonator as shown in Figures 16(a) and 17(a) ($D_L/D_v = 2$). For relatively wide separation between the vias ($D_L/D_v > 4$), the fields near the via-array walls fringe outside the resonator as shown in Figures 16(b) and 17(b). It means that if the geometrical dimen-

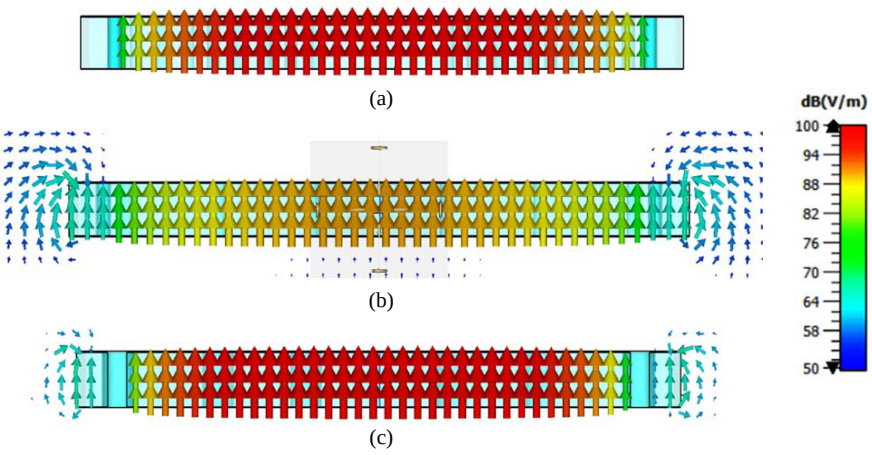

FIGURE 16. The electric field distribution in the vertical section of the SIW resonator near the plane of symmetry when the resonator is excited in the resonance mode TE_{101} for different dimensions of the via-array walls. The resonator has the dimensions listed in Table 2 except for D_v and D_L. (a) $D_v = 0.4$ mm and $D_L = 0.8$ mm, (b) $D_v = 0.4$ mm and $D_L = 2.8$ mm, (c) $D_v = 1.0$ mm and $D_L = 2.8$ mm.

TABLE 4. Dimensions of the fabricated box-shaped resonator embedded in the dielectric substrate; see Figure 3.

Parameter	W	L	h	L_F	W_F
Value (mm)	12.2	18.0	1.57	19.2	3.62

TABLE 5. Dimensions of the fabricated SIW resonator with via-array side walls; see Figure 4.

Parameter	W	L	h	D_v	D_L	L_F	W_F	W_s	L_s
Value (mm)	12.5	18.3	1.57	1.0	3.25	19.2	3.62	16.42	24.0

sions of the resonator (W, L) are being fixed while increasing the ratio D_L/D_v, the effective dimensions of the resonator (W_{eff}, L_{eff}) will be increased to give room for the fringing field. In other words, with increasing the ratio D_L/D_v, the fringing field occupies a larger area leading to effectively increase the resonator area, and hence, $W_{eff} > W$ and $L_{eff} > L$ for $D_L/D_v > 4$. On the other hand, as long as there is no fringing field (i.e., the condition $D_L/D_v < 4$ is satisfied), the effective dimensions are smaller than the geometrical dimensions of the resonator ($W_{eff} < W$ and $L_{eff} < L$).

8. FABRICATION AND EXPERIMENTAL INVESTIGATION

Two prototypes of the resonator under investigation are fabricated and subjected to experimental measurements. The first prototype is for a box-shaped resonator with solid side walls. The second prototype is for a SIW resonator with the conventional via-array side walls. Both the resonators are embedded in a dielectric substrate of the same material and thickness and designed to resonate at the same frequency (10 GHz). The purpose of the experimental work is to investigate the accuracy of the design equations (19) proposed in the present work.

8.1. Fabrication of the Resonators

The substrate material is Rogers RO5880 with $\epsilon_r = 2.2$, loss tangent $\tan\delta = 0.0009$, and height $h = 1.57$ mm. Both of the resonators are designed to be fed through a microstrip transmission line as explained in Section 4. The design parameters of the two resonators are shown in Figures 3 and 4. From (2), a box-shaped resonator of dimensions $W_b = 12.2$ mm and $L_b = 18.0$ mm has a resonant frequency $f_{101} = 10$ GHz. To get the dimensions of the SIW resonator of via-array side walls that resonates at the same frequency (10 GHz), formulas (19), proposed in the present work, can be applied by setting the effective dimensions appearing on the right-hand side to be equal to the dimensions of the box-shaped resonator that resonates at 10 GHz. Consequently, for via diameter, $D_v = 1.0$ mm, and distance $D_L = 3.25$ mm between the vias, the application of (19) with $W_{eff} = W_b = 12.2$ mm and $L_{eff} = L_b = 18.0$ mm gives $W = 12.5$ mm and $L = 18.3$ mm, respectively. Thus, the dimensions of the fabricated box-shaped and SIW resonators are listed Tables 4 and 5, respectively.

The SIW resonator is fabricated using the conventional via-holes to construct the four side walls of the resonator. The box-shaped resonator is more difficult to implement as it requires solid side walls. The procedure applied to fabricate the box-shaped resonator with the dimensions listed in Table 4 on a dielectric substrate of the material RO5880 as mentioned above is illustrated in Figure 18 and can be briefly described as follows. (i) A rectangular patch with the same external dimensions of the resonator (W_s and L_s) is printed on the dielectric substrate using the well-known lithography technique with the feeding microstrip line as shown in Figure 18(a). (ii) The substrate is cut to fit the dimensions of the resonator as shown in Figure 18(b). (iii) A groove penetrating the thickness of the substrate is cut at the lower edge of the patch as shown in Figure 18(c) on the two sides of the microstrip line. (iv) A self-adhesive copper foil tape, as that shown in Figure 18(d), is used to cover the side

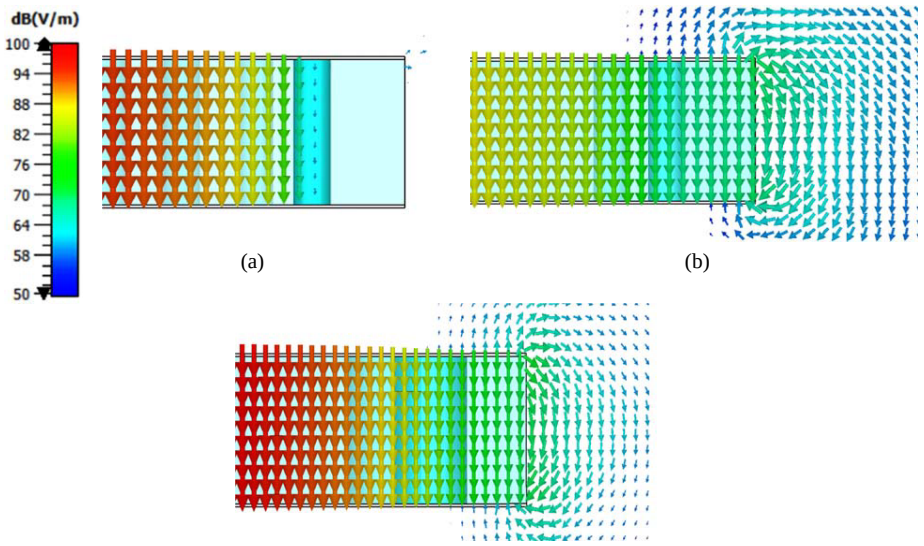

FIGURE 17. Zoomed view of the electric field distribution in the vertical section near the via wall when the resonator is excited in the TE_{101} mode for different dimensions of the via-array walls. The resonator has the dimensions listed in Table 2 except for D_v and D_L. (a) $D_v = 0.4$ mm, $D_L = 0.8$ mm, (b) $D_v = 0.4$ mm, $D_L = 2.8$ mm, (c) $D_v = 1.0$ mm, $D_L = 2.8$ mm.

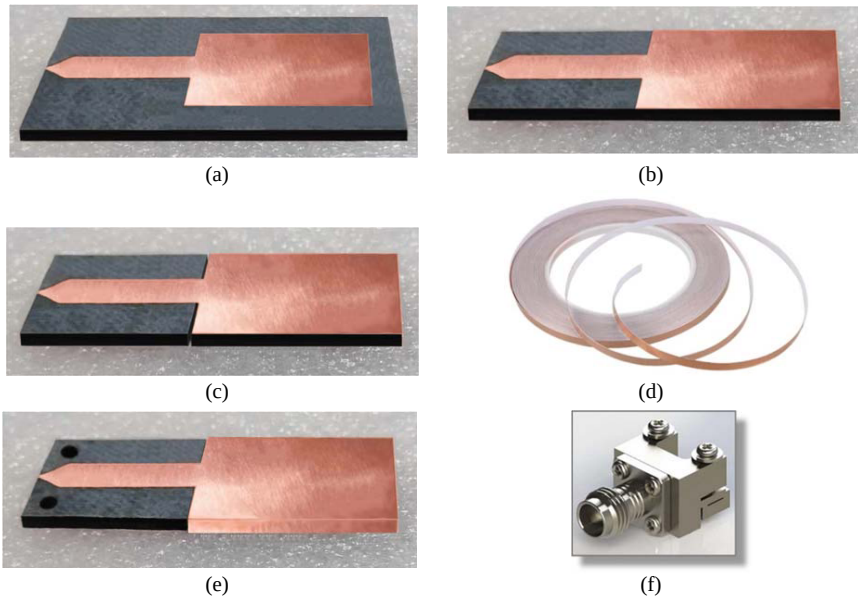

FIGURE 18. Steps of adding the solid side walls to form the box-shaped resonator embedded in the dielectric substrate. (a) A rectangular patch with the resonator dimensions is printed on the dielectric substrate. (b) The substrate is cut to fit the dimensions of the resonator. (c) A groove penetrating the thickness of the substrate is cut at the lower edge of the patch. (d) Self-adhesive copper foil tape. (e) The side surfaces of the substrate are covered with the copper foil tape. (f) The coaxial end-launcher to be mounted on the substrate to excite the resonator.

faces of the resonator as shown in Figure 18(e). (v) Finally, two holes are perforated in the substrate to mount a coaxial end-launcher, as shown in Figure 18(f), for feeding the box-shaped resonator through the printed microstrip line.

8.2. Experimental Measurements

The fabricated box-shaped and SIW resonators are presented in Figures 19(a) and 19(b), respectively. The resonators are subjected to experimental assessment to measure the frequency response of the reflection coefficient magnitude, $|S_{11}|$, using the vector network analyzer (VNA) N9918A so as to determine the resonant frequency of the TE_{101} experimentally and to judge the proposed formulas (19). The connections of the resonators to the VNA are shown in Figure 18. A calibration process is applied to the VNA before the measurement using the calibration kit 85521. The frequency responses of $|S_{11}|$ are, also, obtained by the CST® simulator for comparison with the experimental results. The measured frequency responses of $|S_{11}|$ are compared to those obtained by simulation as shown in Figures 20(a) and 20(b) for the box-shaped and SIW resonators, respectively, showing good agreement. It is shown by simulation as well as by experiment that the resonant frequency is at 10 GHz with excellent accuracy. These results prove the correctness and ac-

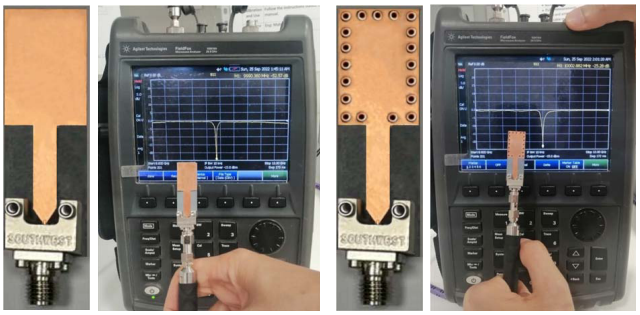

(a) (b)

FIGURE 19. Fabricated prototypes of the substrate-embedded resonators (a) box-shaped resonator, and (b) SIW resonator. Both the resonators are connected to the VNA N9918A for measurement of the reflection coefficient ate the antenna feeding port.

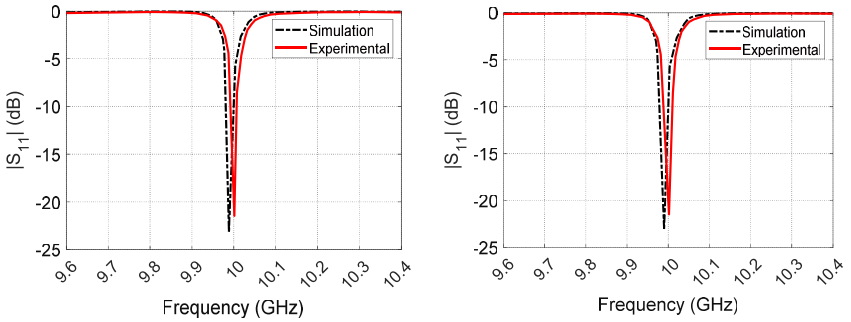

FIGURE 20. Frequency response of the reflection coefficient magnitude, $|S_{11}|$, obtained by simulation and measurement for (a) box-shaped resonator of solid walls, and (b) SIW resonator of via-array side walls.

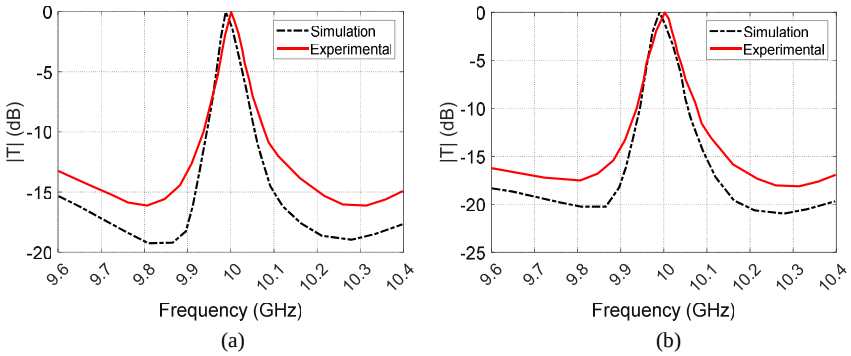

FIGURE 21. Frequency response of the transmission coefficient magnitude, $|T|$, obtained by simulation and measurement for (a) box-shaped resonator of solid walls, and (b) SIW resonator of via-array side walls.

TABLE 6. The resonant frequencies and the corresponding Q-factors.

Resonator Type	Simulation		Measurement	
	f_{101} (GHz)	Q-factor	f_{101} (GHz)	Q-factor
Box-shaped	9.988	238	9.990	230
SIW	10.001	200	10.002	193

curacy of the SIW resonator design equations (19) proposed in the present work.

Figure 21 presents the frequency responses of the measured transmission coefficients, $|T|$, obtained from $|S_{11}|$ at the excitation ports of the two types of resonators by (20). The resonant frequencies and Q-factors obtained by measurement and simulation are listed in Table 6. The measurements are compared to the simulation results showing good agreement in both the f_{101} and the Q-factor. It is shown that Q-factor of the box-shaped resonator is higher than the SIW resonator due to the radiation loss existing in the latter. It should be noted that the Q-factor of the SIW cavity resonator is investigated in many recent publications such as [27–29] for its significance as important design

TABLE 7. Comparison among the performance parameters of SIW cavity resonators proposed in some publications.

Work	Dimensions mm × mm × mm	f_{101} (GHz)	Minimum $\lvert S_{11}\rvert$ (dB)	−10 dB Bandwidth (MHz)	Unloaded Q-Factor
[8]	15.0 × 15.0 × 1.27	9.3	−20	36	880
[9]	19.0 × 14.0 × 0.50	10	−21	38	815
[14]	100.0 × 35.0 × 0.50	3.2	NA	75	308
[14]	23.3 × 15.1 × 0.254	10	NA	105	265
[14]	8.0 × 6.0 × 0.254	20	NA	63	375
[17]	3.45 × 3.45 × 0.79	27	NA	47	600
[20]	36.8 × 36.8 × 1.27	4	−20	48	575
[20]	15.4 × 15.4 × 1.27	10	−19	45	635
[27]	20.0 × 18.0 × 1.3	10	−19.5	35	1609
[Present]	16.5 × 12.4 × 1.57	10	−23	20	2257

parameter (of such type of resonator) when used for various applications.

9. COMPARISON WITH PUBLISHED WORK

A comparison among the performance parameters of SIW cavity resonators proposed in some publications is presented in Table 7. It is shown that the SIW resonator proposed in the present work has the highest Q-factor and the minimum volume among those SIW resonators with $f_{101} = 10$ GHz. However, the main disadvantage of the SIW resonator of the present work is its thicker substrate. It should be noted that a relatively thick substrate is used in the proposed SIW resonator to provide high Q-factor.

10. CONCLUSION

The effects of the dimensions of the via-array side walls on the resonant frequency, radiation loss, and Q-factor of the SIW resonator have been investigated through simulation and experimental work. Two models of the rectangular resonator embedded in a dielectric substrate have been designed to operate at 10 GHz. The first model is an ideal box-shaped resonator of solid side walls whereas the other model is a conventional SIW resonator with via-array side walls. The two types of substrate-embedded resonators are fed through a microstrip line. The resonant frequency, losses, and Q-factor of the two resonator models have been compared to each other taking the box-shaped resonator as a reference because of its ideal structure to evaluate the performance of the conventional SIW resonator. The two types of resonator have been fabricated for comparison through experimental measurements. The empirical design equations commonly available in literature to calculate the effective dimensions of the SIW resonator have been investigated by comparison with the exact simulation results and shown to be incorrect in most cases. More accurate and reliable design equations have been proposed in the present work. The results of the proposed design equations have been compared to the simulation results showing excellent accuracy and being more reliable than those available in literature.

REFERENCES

[1] Hussein, Y. M., M. K. A. Rahim, N. A. Murad, M. M. Jawad, H. O. Hanoosh, H. A. Majid, and H. H. A. Keriee, "Substrate integrated waveguide and microstrip antennas at 28 GHz," *Bulletin of Electrical Engineering and Informatics*, Vol. 9, No. 6, 2462–2468, 2020.

[2] Donelli, M., S. K. Menon, G. Marchi, V. Mulloni, and M. Manekiya, "Design of an ultra wide band antenna based on a SIW resonator," *Progress In Electromagnetics Research C*, Vol. 103, 187–197, 2020.

[3] El Khamlichi, D., N. A. Touhami, T. Elhamadi, and I. Badaoui, "Broadband antenna SIW for X-band application," in *International Conference Interdisciplinarity in Engineering*, Vol. 46, 808–813, 2020.

[4] Miligy, A., A. Hussein, H. Nadir, and M. Rizk, "Investigation and implementation of integrated SIW system for hexagonal diamond of Lamda shape slots fractal array antenna for X and Ku-band applications," *International Journal of Telecommunications*, Vol. 1, No. 1, 1–25, 2021.

[5] Al-Fadhali, N., H. Majid, and R. Omar, "Multiband frequency reconfigurable substrate integrated waveguide antenna using copper strip for cognitive radio applicable to internet of things application," *Telecommunication Systems*, Vol. 76, No. 3, 345–358, Mar. 2021.

[6] Usman, M., E. Kobal, J. Nasir, Y. Zhu, C. Yu, and A. Zhu, "Compact SIW fed dual-port single element annular slot MIMO antenna for 5G mmWave applications," *IEEE Access*, Vol. 9, 91 995–92 002, 2021.

[7] Serhsouh, I., M. Himdi, H. Lebbar, and H. Vettikalladi, "Reconfigurable SIW antenna for fixed frequency beam scanning and 5G applications," *IEEE Access*, Vol. 8, 60 084–60 089, 2020.

[8] Ahmed, R., S. Bri, and M. Sabbane, "Analysis of substrate integrated waveguide (SIW) resonator and design of miniaturized SIW bandpass filter," *International Journal of Electronics and Telecommunications*, Vol. 63, No. 3, 2017.

[9] Grine, F., T. Djerafi, M. T. Benhabiles, K. Wu, and M. L. Riabi, "High-Q substrate integrated waveguide resonator filter with dielectric loading," *IEEE Access*, Vol. 5, 12 526–12 532, 2017.

[10] Hirokawa, J. and M. Ando, "Single-layer feed waveguide consisting of posts for plane TEM wave excitation in parallel plates," *IEEE Transactions on Antennas and Propagation*, Vol. 46, No. 5, 625–630, May 1998.

[11] Cassivi, Y., L. Perregrini, P. Arcioni, M. Bressan, K. Wu, and G. Conciauro, "Dispersion characteristics of substrate integrated

rectangular waveguide," *IEEE Microwave and Wireless Components Letters*, Vol. 12, No. 9, 333–335, Sep. 2002.

[12] Xu, F. and K. Wu, "Guided-wave and leakage characteristics of substrate integrated waveguide," *IEEE Transactions on Microwave Theory and Techniques*, Vol. 53, No. 1, 66–73, Jan. 2005.

[13] Rayas-Sanchez, J. E. and V. Gutierrez-Ayala, "A general EM-based design procedure for single-layer substrate integrated waveguide interconnects with microstrip transitions," in *2008 IEEE MTT-S International Microwave Symposium Digest*, 983–986, IEEE, Atlanta, Ga, Jun. 2008.

[14] Che, W., D. Wang, L. Xu, and C. Li, "Investigation on quality factor of substrate-integrated waveguide resonance cavity," *Microwave and Optical Technology Letters*, Vol. 49, No. 8, 2007–2010, Aug. 2007.

[15] Che, W., K. Deng, D. Wang, and Y. L. Chow, "Analytical equivalence between substrate-integrated waveguide and rectangular waveguide," *IET Microwaves, Antennas & Propagation*, Vol. 2, No. 1, 35–41, 2008.

[16] Deslandes, D. and K. Wu, "Accurate modeling, wave mechanisms, and design considerations of a substrate integrated waveguide," *IEEE Transactions on Microwave Theory and Techniques*, Vol. 54, No. 6, 2516–2526, Jun. 2006.

[17] Bozzi, M., M. Pasian, L. Perregrini, and K. Wu, "On the losses in substrate-integrated waveguides and cavities," *International Journal of Microwave and Wireless Technologies*, Vol. 1, No. 5, 395–401, 2009.

[18] Bozzi, M., L. Perregrini, and K. Wu, "Modeling of conductor, dielectric, and radiation losses in substrate integrated waveguide by the boundary integral-resonant mode expansion method," *IEEE Transactions on Microwave Theory and Techniques*, Vol. 56, No. 12, 3153–3161, Dec. 2008.

[19] Grine, F., T. Djerafi, M. T. Benhabiles, K. Wu, and M. L. Riabi, "High-Q substrate integrated waveguide resonator filter with dielectric loading," *IEEE Access*, Vol. 5, 12 526–12 532, 2017.

[20] Delmonte, N., M. Bozzi, L. Perregrini, and C. Tomassoni, "Miniaturization and quality-factor in substrate integrated waveguide cavities," in *2018 IEEE MTT-S International Conference on Numerical Electromagnetic and Multiphysics Modeling and Optimization (NEMO)*, 1–4, IEEE, 2018.

[21] Deslandes, D., "Design equations for tapered microstrip-to-substrate integrated waveguide transitions," in *2010 IEEE MTT-S International Microwave Symposium Digest (MTT)*, 704–707, IEEE, Anaheim, Ca, May 2010.

[22] Cheng, D. K., *Field and Wave Electromagnetics*, Pearson Education India, 1989.

[23] Pozar, D. M., *Microwave Engineering*, 3rd ed., John Wiley & Sons, Inc., 2005.

[24] Raju, G. S. N., *Electromagnetic Field Theory and Transmission Lines*, Pearson Education India, 2006.

[25] Jordan, E. C. and K. G. Balmain, *Electromagnetic Waves and Radiating Systems*, Prentice Hall, Englewood Cliffs, New Jersey, 1968.

[26] Bozzi, M., A. Georgiadis, and K. Wu, "Review of substrate-integrated waveguide circuits and antennas," *IET Microwaves Antennas & Propagation*, Vol. 5, No. 8, 909–920, Jun. 2011.

[27] Akkader, S., H. Bouyghf, and B. A., "Unloaded quality factor optimization of substrate integrated waveguide resonator using genetic algorithm," *IJECE*, Vol. 13, 2857, 2023.

[28] Lin, G. and Y. Dong, "A compact, hybrid SIW filter with controllable transmission zeros and high selectivity," *IEEE Transactions on Circuits and Systems II: Express Briefs*, Vol. 69, No. 4, 2051–2055, Apr. 2022.

[29] Varcheh, H. N., P. Rezaei, and S. Kiani, "Planar substrate integrated waveguide-based resonators and its usage to compact X-band small phase noise oscillator," *Microwave and Optical Technology Letters*, Vol. 65, No. 1, 54–61, Jan. 2023.